BOREAL ENVIRONMENT RESEARCH 18: 37–52
ISSN 1239-6095 (print) ISSN 1797-2469 (online)

Helsinki 31 January 2013

Modeling and tracer release experiment on forced buoyant plume convection from coastal oxygenation

Jørgen Bendtsen[1)]*, Karin E. Gustafsson[1)], Jouni Lehtoranta[2)], Erkki Saarijärvi[3)], Kai Rasmus[2)4)] and Heikki Pitkänen[2)]

[1)] *VitusLab, Symbion Science Park, Fruebjergvej 3, P.O. Box 98, DK-2100 Copenhagen O, Denmark (*corresponding author's e-mail: jb@vituslab.dk)*
[2)] *Finnish Environment Institute, Marine Research Center, P.O. Box 140, FI-00251 Helsinki, Finland*
[3)] *Vesi-Eko Oy, Yrittäjäntie 12, FI-70150 Kuopio, Finland*
[4)] *Finnish Environment Institute, Freshwater Center, Survontie 9, FI-40500 Jyväskylä, Finland*

Received 22 Sep. 2011, final version received 7 May 2012, accepted 7 May 2012

Bendtsen, J., Gustafsson, K. E., Lehtoranta, J., Saarijärvi, E., Rasmus, K. & Pitkänen, H. 2013: Modeling and tracer release experiment on forced buoyant plume convection from coastal oxygenation. *Boreal Env. Res.* 18: 37–52.

Mechanical oxygenation has been suggested as means of reducing unwanted effects from hypoxia but the near-field dynamics and thereby the potential impact from large scale applications is poorly understood. We present results from a field experiment and model study where the dynamics close to an oxygenator in a shallow coastal area in the Gulf of Finland were studied. The oxygenator created a buoyant plume by pumping surface water through a pipe into the bottom water at a rate of about 1 m^3 s^{-1}. A passive tracer (rhodamine) was added to the inlet of the pump and its lateral spreading was subsequently observed in a relatively thin layer below the pycnocline. The dispersion of rhodamine was applied to parameterize the entrainment rate in a plume model and the total outflow was increased by a factor of about 7. A sensitivity study with different pump rates and cross flow velocities were analysed.

Introduction

Eutrophication deteriorates water quality due to elevated levels of phytoplankton biomass and also leads to increased respiration and, in general, a low oxygen concentration in the deeper part of the water column. Hypoxia ($O_2 < 2$ mg l^{-1}) and anoxia, therefore, characterize many lakes and coastal areas where "ventilation" by oxygen-rich water from the surroundings cannot provide enough oxygen for the mineralisation of organic matter. Depletion of oxygen is lethal to higher organisms and therefore leads to a significant loss of biodiversity in aquatic systems. In sulphate rich systems, low oxygen concentrations may also block the iron cycle and cause a release of iron-bound phosphorus from the sediment (Lehtoranta *et al*. 2008). Release of phosphorus lowers the ratio of dissolved inorganic N to P (DIN:DIP) which, in turn, favours blue-green algal blooms. In addition, anoxia and the presence of hydrogen sulphide (H_2S) limits nitrification (Joye and Holligbaugh 1995) and reduced nitrate supply in turn reduce denitrification processes and thereby the removal of nitrogen from the system (Tuominen *et al*. 1998). These direct and indirect effects of hypoxia and anoxia can be decreased through environmental management

Editor in charge of this article: Andreas Lehmann

strategies which promote reductions of external nutrient loads and counteract eutrophication (Pitkänen *et al*. 2007). Engineering solutions have also been considered as a way to obtain an improvement of the environment. Mechanical oxygenation has been carried out successfully in many Finnish lakes where pumping of oxygen-rich surface water into the hypolimnion has increased the oxygen concentration (Lappalainen 1994). Also pumping of O_2 into the water column has been applied successfully in lakes (Liboriussen *et al*. 2009). Experiences from lakes have led to suggestions of establishing similar solutions in the open sea, and preliminary estimates of the environmental and economic consequences have argued for the feasibility of such solutions for the Baltic Sea region (Stigebrandt and Gustafsson 2007). Thereby mechanical oxygenation could support environmental management plans for nutrient load reductions and speed up improvement of the marine environment as compared with effects of nutrient reductions from land alone, where first significant improvements may be expected after several years or decades after they had been implemented due to the long residence time of nutrients in the sea.

Previous studies of oxygenation considered both a method with direct pumping of surface water into the water column and a method of pumping air or O_2 where the subsequent bubble formation also causes a rising buoyant plume. Pumping of air (in comparison with pure oxygen gas), in principle, may have negative consequences for fish due to the dissolution of N_2. However, this effect has not been found to be significant (Gafsi *et al*. 2009). Although the dynamics inside the rising buoyant plume is different between the two methods the general plume dynamics is similar. The formation of a buoyant bubble plume from pumping air or pure oxygen into a stratified water column has been analysed through integral plume models where the conditions within the plume consider phase changes together with the entrainment of surrounding water into the plume (McDougall 1978, Wüest *et al*. 1992). Measurements of near-field (~10 m) and far-field (10~1000 m) conditions of temperature and velocity fields were analysed close to a bubble plume located in a deep lake and it was shown that an integral plume model could account for the plume characteristics, such as plume temperature and width (McGinnis *et al*. 2004). A one-dimensional plume model has been applied in lakes where horizontally homogeneous layers are ventilated through vertical mixing from a plume forced by bubbles or surface water pumped deep into the water column (Moshfeghi *et al*. 2005). These models are based on a relatively simple parameterization of the entrainment of surrounding water into the rising plume where entrainment rates are determined by buoyancy differences between the plume and surrounding water. Such parameterization of entrainment processes is in accordance with laboratory studies of plume dynamics in stratified environments (Turner 1979). Similar parameterizations have been applied in atmospheric modelling of dispersion of pollutants from point sources or in modeling of pollutants from waste water outlets in the sea. Integral models provide detailed information about the general dynamics inside the plume but only limited information on the far-field dynamics which is of main interest when the influence from artificial oxygenation is considered in the open ocean. The far-field response from plume dynamics has been studied around hydrothermal vents in the deep ocean (Lavelle 1995), and also high resolution plume dynamical models have been coupled to a far-field circulation model (Choi and Lee 2007). However, the understanding of the far-field influence of a rising buoyant plume in the water column is still limited. Entrainment and the influence from detrainment and lateral spreading at the top level of the plume depends on turbulent viscous and diffusive fluxes and these processes are difficult to describe satisfactorily in ocean circulation models.

To assess the potential of oxygenation in the open sea and to understand the primary physical transports caused by a buoyant plume we investigated the dynamics around a buoyant plume through intense measurements during a short term field experiment in a coastal area where a passive tracer was released within an oxygenator. We used the high-spatial resolution data to constrain the parameters in a new simple buoyant plume model suitable for implementation in large scale regional circulation models. We first describe the tracer field experiment and the

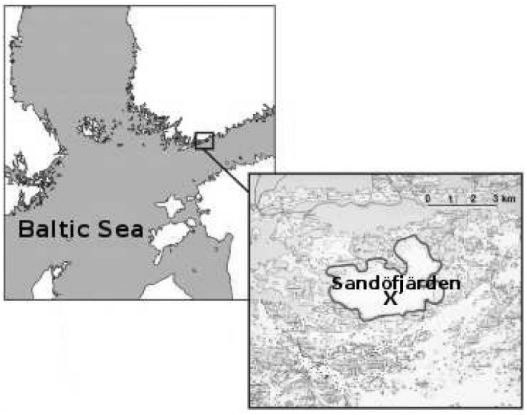

Fig. 1. The map of Sandöfjärden and its location in the northwestern part of the Gulf of Finland. The oxygenator was located in the centre of Sandöfjärden (marked with an X).

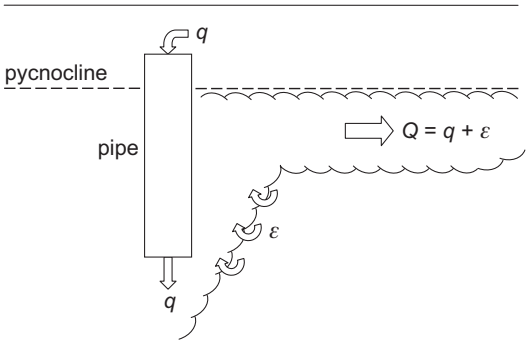

Fig. 2. A scheme of the oxygenator. The oxygenator pumps surface water into the bottom layer with a constant flow rate (q). Surface water with a relatively low density rises as a buoyant plume and entrains surrounding water (ε). The plume reaches its top level and spreads out laterally (Q) below the pycnocline.

buoyant plume model. We analyse the data and use the observations to constrain a free parameter in the plume model. Finally, we apply the model to determine the importance of stratification, flow rate and the far-field currents for the lateral dispersion at the top level of the plume and discuss the application of oxygenation on larger scales.

Methods

Rhodamine experiment

An intense short-term field experiment was carried out on 3 August 2010 in Sandöfjärden located in the southern Finnish archipelago close to the entrance to the Gulf of Finland (Fig. 1). Sändöfjärden has a maximum depth of about 30 m and is a semi-enclosed area with openings towards the Gulf of Finland to the south and to the surrounding archipelago through shallow sills with depths down to 12 m. The deepest part of the basin has a relatively small exchange of bottom water with the surrounding areas and is characterized by late summer–early autumn anoxia in the bottom water. The field experiment was designed to determine the dynamics around a buoyant plume driven by pumping water from 3 m below the surface down to a depth of 17 m through a 0.8 m wide pipe with a Mixox oxygenator. The Mixox oxygenator pumps water through a pipe formed by a thick plastic canvas with a large propeller mounted at the top. The propeller sustains a relatively constant flow rate of about 1 m^3 s^{-1}. Such pumping devices have been used in many Finnish lake areas for mechanical oxygenation of the bottom water (Lappalainen 1994). The circulation close to the oxygenator can conceptually be described by the downward pumping of surface water at a constant flow rate (q) causing an ascending buoyant plume from the pipe outlet and the resultant entrainment (ε) causes a significant increase of the volume flow and the detrainment and lateral spreading ($Q = q + \varepsilon$) occurs at the level of neutral buoyancy between the plume and the surroundings, below the pycnocline (Fig. 2).

Measurements of temperature, salinity, oxygen and rhodamine were made on a closely spaced sampling grid within a distance of 300 m from the pump. Minimal external disturbance of the water column was required during the experiment and, therefore, two 100-m-long ropes were placed in a shape of a N–S and E–W cross with the pump in the centre. Floats were placed as markers along the lines at 10-m intervals. Two boats were operating during the experiment and they were manoeuvred manually without engines along the ropes to reduce mixing in the surface layer. At distances larger than 50 m from the pump the boats were manoeuvred by small engines. The area had been influenced by the

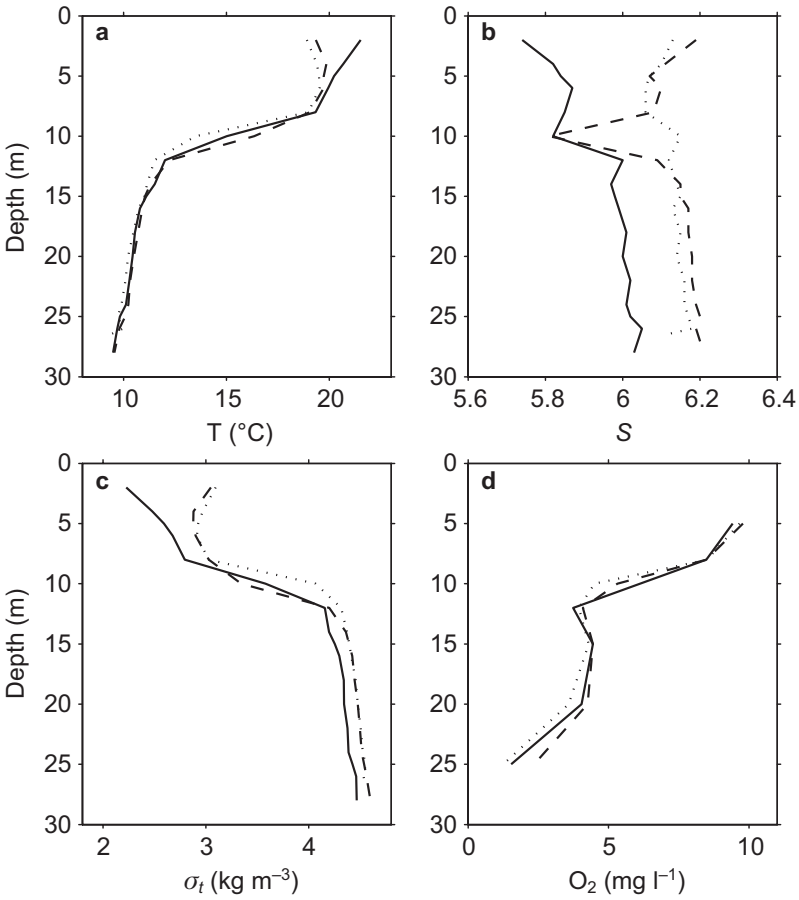

Fig. 3. Initial fields of (**a**) temperature, (**b**) salinity, (**c**) σ_t and (**d**) O_2. Profiles from the YSI profiler are measured at a distance of 50 m to the south (solid line), north (dotted line) and west (dashed line), respectively.

pumping from six oxygenators located in the area from the beginning of July until 30 July, when the oxygenators were stopped. A single pump was started on 3 August at 12:03 and a 20% rhodamine solution was added to the intake of the pump at a rate of 1.4 ml s^{-1} from 16:03 to 17:39. Before the addition of rhodamine (13:00–16:00) the initial fields of temperature, salinity and oxygen around the pump were measured within a distance of 50 m (Fig. 3). The seasonal thermocline was located at about 10-m depth, and the temperatures of the surface and bottom waters were of 20 °C and 9.8 °C, respectively. The salinity distribution was weakly stratified with vertical differences between the surface and bottom waters of about 0.4. An oxygen concentration below 4 mg l^{-1} in the bottom water indicated a relatively stagnant water mass. The salinity distribution showed some spatial variability and this was also observed during the experiment, indicating influence from mixing between the different basins in the area. The density change due to the small-scale variation in salinity observed at a distance of 50 m from the oxygenator (Fig. 3b) was compensated by corresponding temperature changes (this could indicate mixing due to small-scale interleaving) so the combined effect on density were small. The initial density difference between the surface water and 20-m depth were about 2 kg m^{-3}.

The supply of rhodamine was arranged from a raft placed above the pump where a small pipe connected a jar on the raft to the intake of the pump. The flow of rhodamine was driven by the hydrostatic pressure difference between the raft and the intake, and the level in the jar was kept nearly constant by continuously adding insoluble material to the jar during the experiment such that the flow rate of rhodamine was approximately constant. The experiment was carried

out during calm weather conditions and the meteorological parameters were measured from a weather station, mounted on a permanent raft station for monitoring the oxygenators, located in the centre of Sandöfjärden. The meteorological forcing parameters during the experiment from 16:00 to 19:30 were (mean ± SD): surface air temperature = 19.3 ± 0.1 °C, wind speed = 3.9 ± 0.8 m s^{-1}, wind direction = 37.5° ± 8.6°, humidity = 84% ± 2%, air pressure = 1008.9 ± 0.7 hPa, precipitation < 0.02 mm (i.e., practically no precipitation) and a cloudiness of 7/8. These observed parameters were used in the numerical simulations, as described below. The wave height was less than 0.1 m.

One boat with a YSI 6130 rhodamine probe and a temperature and conductivity sensor measured along the north–south and the east–west direction at discrete depth levels of 2, 5, 8, 10, 12, 15, 20 and 25 m during the period of 16 to 20 hours. Finally a transect was made at a distance between 70 and 300 m eastward of the pump where the sensors measured continuously at about 8-m depth. The second boat used a TriOS fluorescence and temperature sensor in the upper 16 m and measurements were performed with a relatively high vertical resolution where rhodamine was observed. The two florescence sensors were inter-calibrated before the experiment started. Additional measurements were made during the following two days after the rhodamine was released but no rhodamine was found in the area.

Current measurements were carried out in 2-m intervals in the upper 12 m with the permanent ADCP-sensor located below the permanent raft station. During the experiment from 16:08 to 20:08 the mean (± SD) current speed and its direction at 4–12-m depth were 2.9 ± 0.4 cm s^{-1} and 108° ± 13°, respectively. The current and its direction in the upper 2 m were 5.2 ± 1.6 cm s^{-1} and 113° ± 23°, respectively. Because of the relatively weak currents during the experiment, these were not included in the numerical simulations of the rhodamine experiment. However, the effects from a far-field cross-flow on the plume dynamics was analysed in a sensitivity study (*see* section 'Effects of far-field currents and pump rate').

Model description

Regional model description

The regional model was based on the three-dimensional circulation model COHERENS (Luyten *et al*. 1999). COHERENS is based on the primitive equations, the Boussinesq approximation, assumes hydrostatic balance and applies an f-plane approximation. The model domain covered a region of 500 × 500 m with a horizontal grid spacing of 20 × 20 m and 30 vertical sigma-layers. The vertical mixing was derived from a k-ε turbulence scheme, where a weak vertical background turbulent diffusion coefficient of 10^{-6} m^2 s^{-1} was included. There was no explicit horizontal mixing and a higher order TVD-advection scheme for momentum and tracers was applied to limit numerical diffusion. The initial fields were determined from observations of temperature and salinity before rhodamine was released into the water. The open boundary conditions were determined by a radiation condition for the barotropic mode (i.e. the method of characteristics; Luyten *et al*. 1999). A no-flux condition was assumed for the baroclinic velocity components and a scalar condition, determined from the observed initial conditions, was applied for temperature and salinity. The meteorological forcing parameters were assumed constant during the experiment and the model was forced by the observed mean values described above.

Plume model description

A new buoyant plume model suitable for implementation in a regional circulation model was developed, and it was coupled to the setup of the COHERENS model described above. The buoyant plume model was assumed to be located within a single horizontal grid cell in the regional model. In a large scale regional setup the horizontal scales could be of the order of about 1–10 km, but for the field experiment a high resolution setup was applied with a horizontal grid resolution of only 20 m. However, even on a fine resolution horizontal grid of 20 m, the plume dynamics is expected to take place on

a much smaller spatial scale and therefore the mixing and transport associated with the plume can be considered a subgrid-scale process. The coupling of the plume model with a regional circulation model calculates the exchange of substances between the plume and the surroundings explicitly, as described below.

The plume model permanently covers a water column from the bottom ($z = -H$) to the surface ($z = \eta$) and mass in the plume is conserved through the continuity and transport equations (Eqs. 1 and 2, respectively) for the various dissolved substances transported through the plume:

$$\frac{\partial u_p}{\partial x} + \frac{\partial v_p}{\partial y} + \frac{\partial w_p}{\partial z} = 0 \quad (1)$$

$$\frac{\partial \phi_p}{\partial t} + \frac{\partial \phi u_p}{\partial x} + \frac{\partial \phi v_p}{\partial y} + \frac{\partial \phi w_p}{\partial z} + A_h\left(\boldsymbol{U}_h, \Phi, \phi_p\right) = 0 \quad (2)$$

where u_p, v_p, w_p are the velocity components in the plume, and ϕ_p is the tracer concentration in the plume. The transport between the surrounding grid and the plume is described by the advection operator $A_h(\boldsymbol{U}_h, \Phi, \phi_p)$ where $\boldsymbol{U}_h$ is the horizontal (far-field) velocity vector in the surrounding grid, and Φ and ϕ_p are the tracer concentrations in the surrounding grid and in the plume, respectively. The plume is assumed to cover a small area (δa) which is significantly smaller than the area of the surrounding grid cell (δA) and the timescale for substances in the plume area is assumed to be sufficiently short such that additional sink or source terms can be neglected in Eq. 2. The assumption that the plume covers a relatively small area is a reasonable approximation when the plume model is implemented in regional models with significantly larger grid sizes than in the current setup. The plume model is assumed to have a constant volume $V_0 = \delta a(t)H_0(t)$, where changes in water level (H_0) are compensated by changes in the surface area of the plume. Horizontal transports between the surrounding grid and the plume grid are determined by an upwind scheme.

The buoyant plume model considers the inflow to the oxygenator and the outflow is represented as a point source of buoyancy and dissolved substances. The buoyancy flux (F) at the bottom of the pipe is determined from the flow rate through the pipe (π_0) and the buoyancy as: $F = \pi_0 B$, where the buoyancy is given by $B = g(\varrho_0 - \varrho_p)/\varrho_0$. The densities ϱ_p and ϱ_0 represent the density in the plume and in the surrounding water, respectively, and g is the acceleration of gravity. The water is assumed to ascend when $B > 0$ and the entrainment of surrounding water then depends on the horizontal buoyancy difference and the height (z_p) above the buoyancy source. From dimensional analysis the entrainment transport can be related to F and z_p as (Turner 1979):

$$\varepsilon = \varepsilon_0 F^{1/3} z_p^{-1/3} \quad (3)$$

where ε_0 is the entrainment parameter to be determined below. Detrainment is assumed to take place at the plume top level where $B \le 0$. A compensating return flow (γ_k) for balancing the entrainment from the "regional" grid cell where the plume is located, is assumed below the detrainment depth level and, correspondingly, a return flow of π_0 is assumed to take place towards the intake of the pipe (Fig. 4). The compensating return flow due to the entrainment and pump intake results in a local mass balance within a single vertical column in the regional model. The compensation flow will depend on turbulent viscosity and diffusion intensities around the pump inlet and this return flow would therefore be expected to occur on a relatively large horizontal scale. In this high resolution setup, the compensating return flow occurs within a short distance of 20 m and this is not expected to be representative for the real flow. However, the compensation flow ensures that there are no net vertically integrated sinks and sources for temperature, salinity and other substances. In a large-scale model application, the return flow becomes correspondingly weaker because of the larger horizontal grid dimensions with typical horizontal scales of $O(10^3)$ m, as discussed further below.

Results

Observed rhodamine distribution

Initially the rhodamine was measured close to

the pump and immediately after the introduction of rhodamine a first section was made in the southward direction within a distance of 50 m from the pump (Fig. 5a). Thereafter, a northward section was measured within a distance of 45 m (Fig. 5b) followed by a westward section (Fig. 5c). In the westward section, rhodamine was only observed within a distance of 40 m from the pump, and this could be explained by the observed weak eastward current. After the end of the rhodamine release an eastward section was measured and the rhodamine was more dispersed and may have been advected away from the pump location (Fig. 5d).

The core of the rhodamine distribution was observed to be centred in and just below the pycnocline in the depth range 10–15 m. An averaged vertical distribution was determined from the measurements for each of the two instruments. The averaged YSI-measurements were calculated from 11 profiles in the four directions (N_{15}, N_{25}, N_{35}, N_{45}, S_{15}, S_{25}, S_{35}, S_{45}, W_{15}, W_{25} and W_{35}, where the index indicate the distance (m) of the station to the oxygenator along each transect). The corresponding averaged vertical profile of the TriOS-measurements was based on 4 profiles (E_{50}, E_{10}, E_{15} and E_{50}) and was binned into 2-m depth intervals in the depth range between 3 and 15 m. The averaged vertical profiles from the YSI-instrument showed a significantly elevated rhodamine concentration at 12–13-m depth of about 21 μg l^{-1} and low average concentrations (< 2 μg l^{-1}) above 10 and below 15-m depth, respectively (Fig. 6a). The TriOS measurements showed a similar increase of rhodamine in the depth range between 10 and 15 m with an average concentration of about 20 μg l^{-1} at 13–15-m depth (Fig. 6b). Finally during the period between 19:00 and 19:30, the rhodamine "cloud" was searched for at a depth of 14 m in a transect from a distance of 300 m east of the pump and towards the pump. Rhodamine concentrations of 1.8 and 32 μg l^{-1} was measured at a distance of 224 m (19:22) and 199 m (19:26), respectively, corresponding to a mean plume velocity of about 88 m h^{-1}.

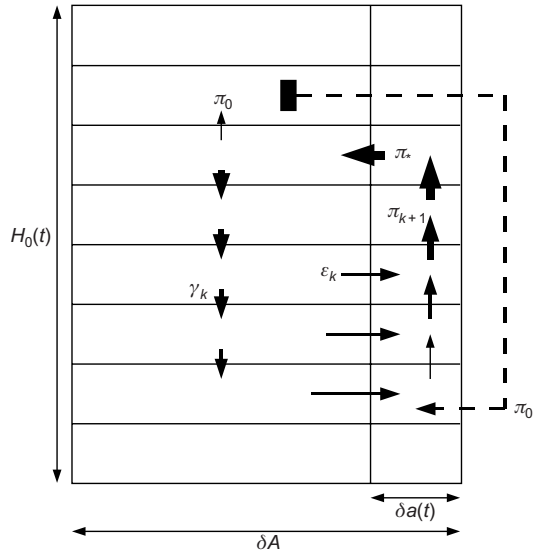

Fig. 4. The buoyant plume model constitutes a constant volume [$V_0 = H_0(t)\delta a(t)$] and the vertical layers are defined by the surrounding grid in the circulation model. The constant flow rate (π_0) transports water from the intake level (k_i) in the regional model to the bottom plume level (k_b). Transport in the plume increases due to entrainment of surrounding water (ε_k) and at the final top level water is transported from the plume to the surroundings. The return flow (γ_k) compensates the transport due to entrainment and the pump intake.

Entrainment parameter

In accordance with the observed distribution of rhodamine we assumed that rhodamine was transported from the bottom pipe outlet within a buoyant plume which reached the top level below the pycnocline. The subsequent lateral dispersion of the rhodamine occurred in a relatively well-defined thin layer with a thickness of about 3 m, corresponding to the observed distribution obtained from the averaged profiles. This implied that the rhodamine distribution close to the oxygenator could be approximated as a steady state distribution after a relatively short period. For example, the residence time of a 3-m-thick circular layer with a radius of 30 m is 2.4 hours if the transport is 1 m^3 s^{-1}. When additional transport from entrained water (about 5–10 m^3 s^{-1}) is taken into account, the residence time of the plume layer is reduced to less than 30 minutes. The observed distribution supported our assumption that the rhodamine distribution could be regarded as being in a steady state close to the oxygenator. The comparison below of the

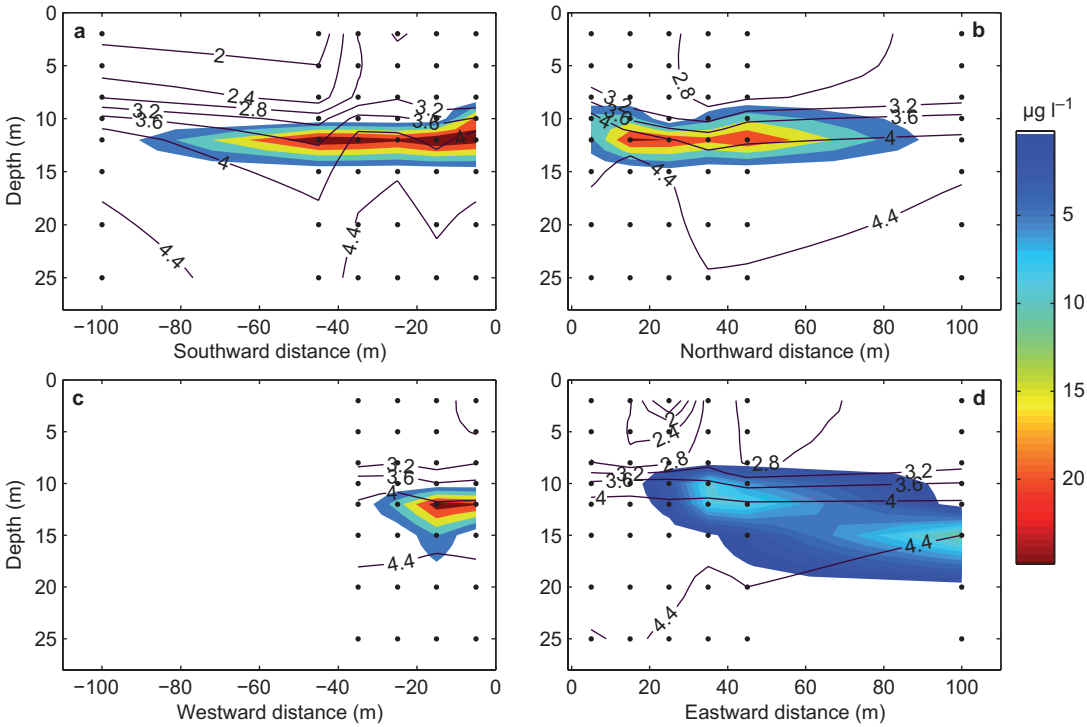

Fig. 5. Rhodamine concentration (μg l^{-1}) along transects towards the (**a**) south, (**b**) north, (**c**) west and (**d**) east. Black lines are contours of constant σ_t (kg m^{-3}). The rhodamine release ended at 17:39 and measurements at the transects started at 16:15 (**b**), 16:52 (**a**), 17:27 (**c**) and 17:54 (**d**).

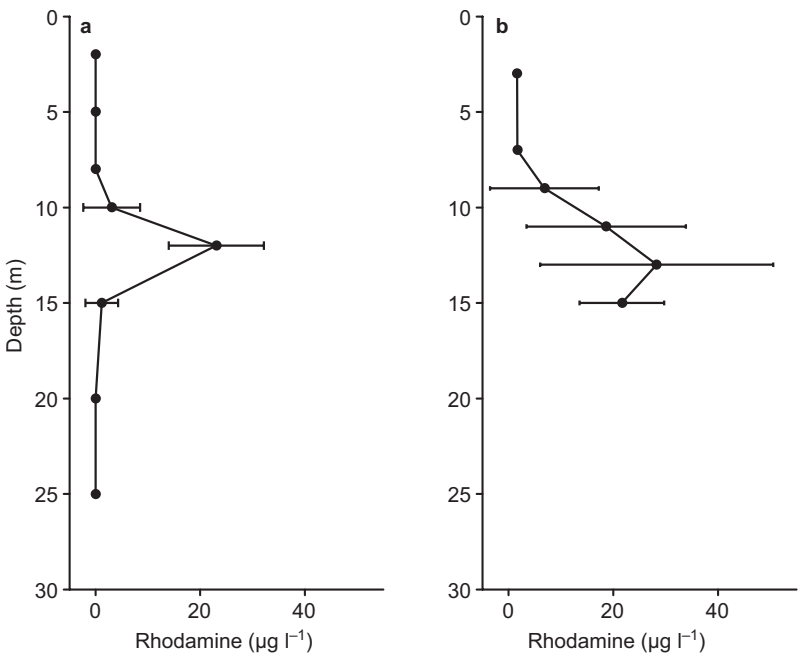

Fig. 6. (**a**) Vertically-averaged distribution of rhodamine (mean ± SD, n = 11, μg l^{-1}) from the YSI measurements, and (**b**) TriOS measurements (mean ± SD, n = 4, μg l^{-1}) within a distance of up to 45 m from the pump.

simulated rhodamine distribution during a short period of 15 minutes, and about 1 hour after the start of the experiment, can therefore be regarded as representative for the steady state rhodamine distribution close to the oxygenator.

The conservation of mass at the intake of the pump requires a compensating inflow from the surroundings, and in the plume model it was assumed to occur locally within the column of grid cells containing the plume. Correspondingly, the local recirculation due to the entrainment into the plume causes a downward transport towards the outlet of the pump (cf. γ_k in Fig. 4). The horizontal scale of the compensating recirculation levels thereby becomes dependent upon the grid size of the model. Few studies of this recirculation around buoyant plumes exist and numerical studies indicate that this recirculation occurs on spatial scales on the order of 10^2–10^3 m (Lavelle 1995) due to the preferential isopychnal transport in the ocean. Therefore, we expect this local recirculation to occur on larger spatial scales than the applied grid size of 20 m, and the local recirculation in the plume model probably becomes more realistic when the horizontal grid resolution increases to ~10^3 m as typically applied in regional scale circulation models. The dynamics of the recirculation is dependent upon the viscous and diffusive turbulent fluxes. However, these are critical processes to describe accurately in regional circulation models and due to the limited data set we therefore do not present a further detailed description of these processes in this study.

The influence of the local recirculation was simulated by considering a case with and without local recirculation of rhodamine, whereas temperature and salinity were recirculated locally in both cases (Fig. 7). The density gradients around the pump caused a weak recirculation which was identical in the two cases. Without local recirculation the rhodamine was confined to a relatively narrow about 3-m-thick layer, whereas the case with recirculation caused a significant amount of rhodamine to be distributed in about a 10-m-thick layer close to the pump in disagreement with the observed distribution (not shown). This simulation suggests that the recirculation occurs on larger spatial scales than the applied 20-m grid resolution, and therefore we disregard the local recirculation of the rhodamine in the direct comparisons between simulations and observations of rhodamine below.

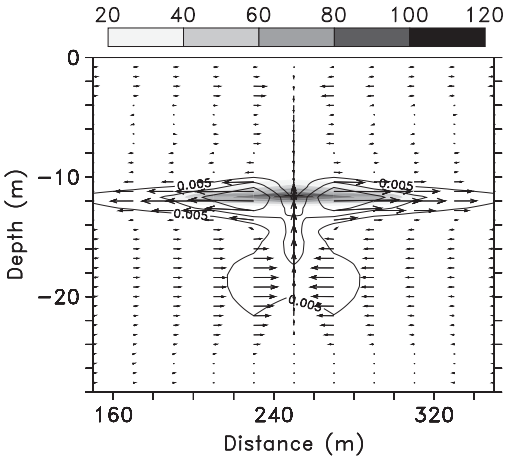

Fig. 7. Distribution of rhodamine in an east–west subsection of the model domain after one hour after the release (scale in μg l^{-1}). Velocity vectors (only every 8th velocity vector is shown in the vertical) and contours of the current speed. The oxygenator is located at a distance of 250 m.

Optimizing the entrainment parameter

The distribution of rhodamine was used for constraining the free entrainment parameter (ε_0) in the buoyant plume model. The model distribution was spatially averaged within a distance of 45 m of the pump and the resultant vertical profile was compared to the observed mean vertical distributions (Fig. 6). The difference between model (C_m) and observations (C_{obs}) was quantified by calculating the residual at each depth level as:

$$R = \sum \frac{\left(C_m - C_{obs}\right)^2}{\sigma_{obs}} \quad (4)$$

where the residual (R) was normalised with the standard deviation at each depth level (σ_{obs}). The residual was determined in an interval of ε_0 between 0.02 and 0.5 (Fig. 8a). A best fit value of ε_0 was determined by the minimum residual value when integrated over the whole water column averaged over a distance of 5–45 m from the oxygenator in the period 17:15–17:30.

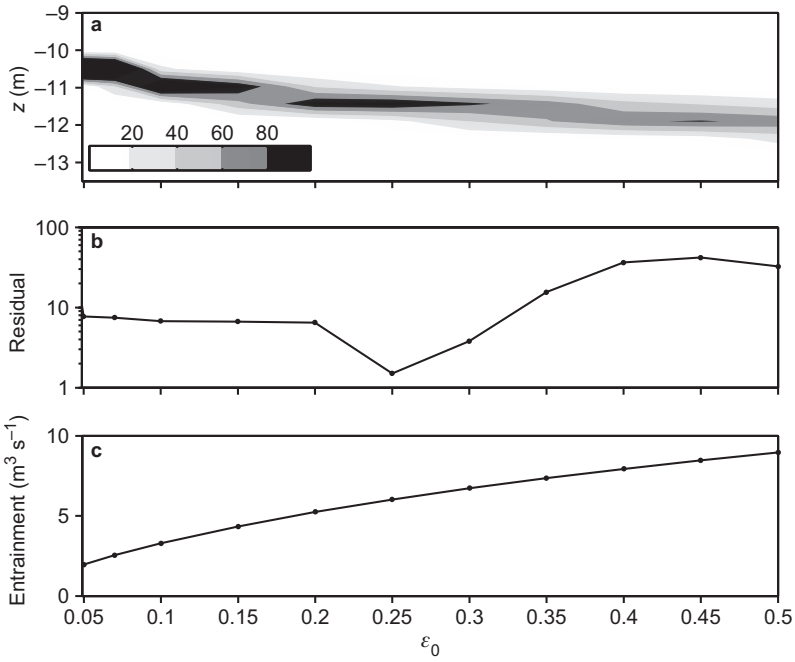

Fig. 8. (**a**) Averaged simulated rhodamine distribution within a distance of 45 m from the oxygenator (scale in μg l^{-1}), (**b**) sum of residuals (R) between observed and simulated averaged vertical profiles of rhodamine concentration, and (**c**) total simulated detrainment flux *versus* the entrainment parameter (ε_0).

In general, the residual decreased in the interval from 0.02 to 0.35 and the best fit value was found at $\varepsilon_0 = 0.25$ (Fig. 8b). Influence from ε_0 on the total detrainment, corresponding to the sum of the vertically integrated entrainment and the pump flow rate, was found to increase gradually from 2 to 9 m^3 s^{-1} in the interval of ε_0 (Fig. 8c). The best fit value of $\varepsilon_0 = 0.25$ caused a total detrainment of 7 m^3 s^{-1} implying that the initial flow rate of 1 m^3 s^{-1} was amplified by a factor of seven due to entrainment of the surrounding water.

Model solutions with the best fit value of ε_0 were vertically integrated and compared with the corresponding observed rhodamine distribution within a distance of 45 m from the pump. The averaged simulated model content of rhodamine of 62 mg m^{-2} was in general accordance with the observed rhodamine distribution (Fig. 9). The model solution showed a gradual decrease of the rhodamine content from 108 mg m^{-2} at a distance of 5 m to 40 mg m^{-2} at 45 m, which would be expected from the radial spreading away from the pump. The observed distribution of rhodamine varied between 63 and 93 mg m^{-2} except for a minimum value of 31 mg m^{-2} observed at the western transect at a distance of 30 m from the pump. This low value was probably due to the small eastward advection in the area. However, the averaged simulated rhodamine content was in general accordance with the observed rhodamine.

A transient model simulation of the experiment showed that after about 15 minutes a significant amount of rhodamine was simulated at a distance of about 40 m from the pump (Fig. 10). After one hour the rhodamine distribution was still within a distance of 100 m from the pump and the highest concentration was centred close to the pump. After the rhodamine release was stopped the simulated rhodamine distribution moved outwards from the pump and the concentration in the rhodamine cloud was reduced due to mixing.

Effects of far-field currents and pump rate

The sensitivity of the plume model to changes in the far-field current field and the total pump rate through the oxygenator was analysed for different values of a constant east–west cross flow velocity (U) and pump rate (Q). Increasing the horizontal velocity from zero to 0.1 m s^{-1} led to a significant decrease in the height of the top level of the plume (Figs. 11 and 12). Doubling

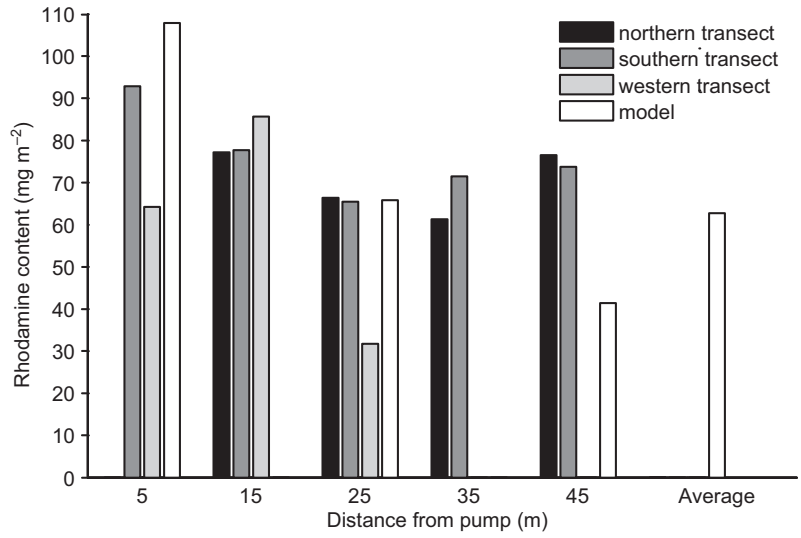

Fig. 9. Vertically integrated rhodamine content in the depth interval between 10 and 15 m from the YSI measurements along the northern (black), southern (dark gray) and western (lightgray) transects. The model solution (ε_0 = 0.25, white) at the corresponding distances averaged in the time interval from 17:15 to 17:30, and the average rhodamine content within a distance of 5 to 45 m from the pump during the same period.

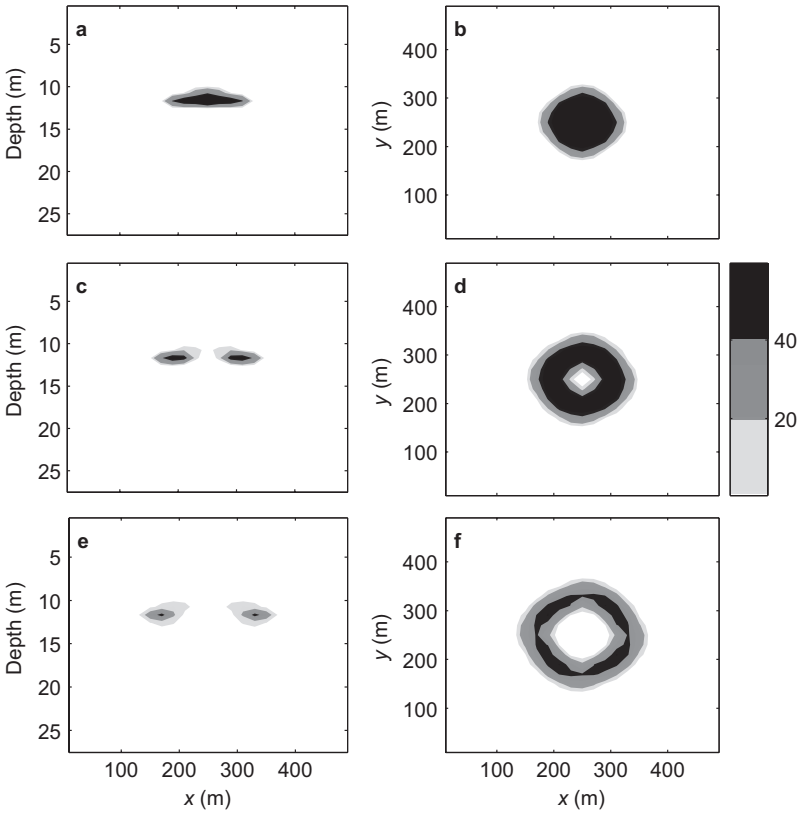

Fig. 10. Model simulations of the rhodamine experiment in a 500 × 500-m and 28-m-deep model domain (grayscale in μg l^{-1}). Solutions of a north–south transect (left-hand-side panels) and the horizontal plane (right-hand-side panels) distributions of rhodamine at 16:15 (**a**, **b**), 17:00 (**c**, **d**) and 18:00 (**e**, **f**).

the pump rate (and the rhodamine flux) reduced the impact from the far-field current field due to the larger buoyancy flux from the oxygenator. The horizontal velocity caused an exchange with the plume at all depth levels and this deepened the rhodamine distribution compared to the relatively thin layer of lateral spreading in the case with no horizontal velocity. Increasing the cross

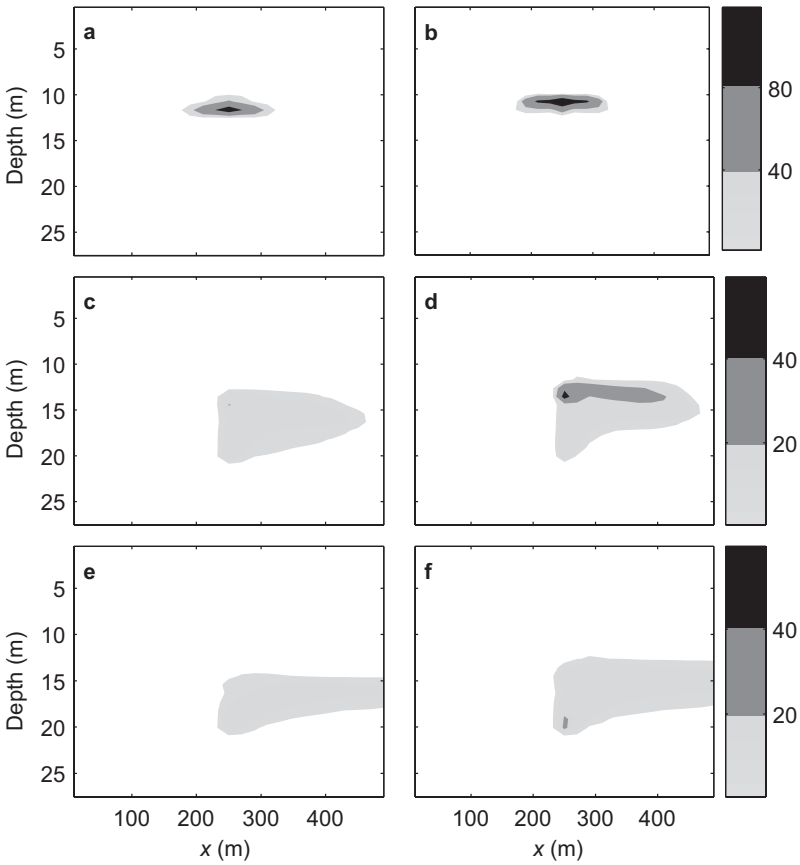

Fig. 11. Model simulations of rhodamine concentrations (grayscale in μg l^{-1}) after one hour of rhodamine release. Left and right panels show model solutions with a flow through the oxygenator (*q*) of 1 and 2 m^3 s^{-1}, respectively. Solutions are shown for a horizontal cross-flow velocity (*u*) of 0 (upper panels), u = 0.05 (middle panels) and u = 0.1 m s^{-1} (lower panels), respectively.

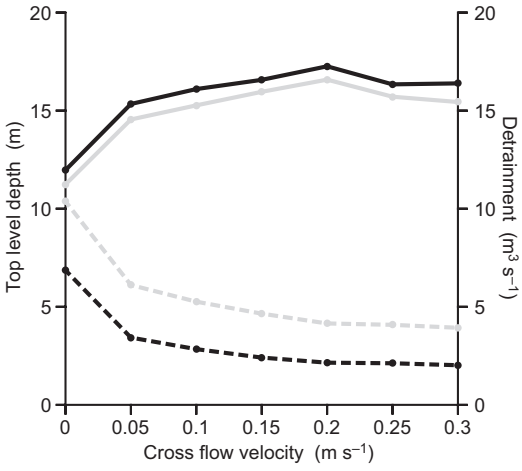

Fig. 12. Model sensitivity to the cross flow velocity. Solutions for the top level (solid lines) and total detrainment from the plume (dashed lines) are shown in two cases with a pump rate of 1 m^3 s^{-1} (black) and 2 m^3 s^{-1} (gray), respectively. The plume source is located at 20-m depth.

flow velocity from zero to 0.3 m s^{-1}, in the case with an oxygenator through flow of 1 m^3 s^{-1}, caused the top level to sink from 12 m to 16.4-m depth while the detrainment decreased from 6.9 to 2.0 m^3 s^{-1} (Fig. 12). In case the flow through the oxygenator was increased to 2 m^3 s^{-1} a corresponding change in the cross-flow velocity from zero to 0.3 m s^{-1} lowered the initial top level of 11.2 m to 15.4 m and the detrainment decreased correspondingly from 10.4 to 3.9 m^3 s^{-1}.

Discussion

The model analysis and the rhodamine experiment provided information on the dynamics close to the oxygenator on a relatively short time scale. However, the environmental benefits from oxygenation would be expected to be seen on larger spatial scales, for example as a general improvement of the bottom water oxygen condi-

tions in the whole Sandöfjärden or even on larger regional scales. Below, we discuss the results in relation to the near-field physical dynamics and also consider how these results could be applied in the design of a larger scale experiment, for example through application of several oxygenators and/or application of oxygenation on larger temporal and spatial scales.

Near-field dynamics and recirculation

Rhodamine was observed in a well-confined layer of water spreading laterally from the pump area, and only minor concentrations of rhodamine were observed above the pycnocline. This observation indicates that the flow associated with plume convection from the pump only transports a very limited amount of bottom water into the surface layer locally, and that the lateral spreading mainly occurs below the pycnocline. Therefore, the potential risk of directly transporting nutrient rich bottom water into the surface layer can be regarded as minimal with the applied flow rate and the observed stratification. This is an important finding, because it shows that the risk of indirectly stimulating a phytoplankton bloom through oxygenation can be considered as small when a significant pycnocline separates surface and bottom water. In this case, the density difference was about 1–2 kg m^{-3} (cf. Fig. 4). Correspondingly, the risk of bringing bottom water with a high concentration of hydrogen sulphide to the surface can be considered to be limited. However, the near-field dynamics showed that even though there were no significant transports across the pycnocline there would still be an upward transport of bottom water substances towards the bottom of the pycnocline. Therefore, bottom water nutrients may induce an increased subsurface primary production or, in the case of hypoxic or hydrogen sulphide rich bottom water, it could lower the sub-pycnocline oxygen concentration. This would also have to be considered if a significant deepening of the mixed layer could occur, for example due to episodic and strong wind forcing.

No significant amount of rhodamine was observed below a depth of 15 m and at a distance of 5 m from the pump. A direct influence from the pumping on the water close to the bottom was therefore not observed during the 4 hours when observations were made. The entrainment of surrounding water into the rising plume will establish a compensating current close to the pump and thereby affect the circulation in the bottom layer. Therefore, a recirculation in the bottom water towards the pump may be significant but the duration of the rhodamine release was probably too short to re-circulate the rhodamine back to the plume area through the bottom layer. Model simulations showed a significant far-field recirculation towards the pump (cf. Fig. 7) induced by the entrainment of water into the rising buoyant plume, and this recirculation would imply a circulation, and therby a ventilation, of deeper parts of the water column. The simulated far-field recirculation is driven by pressure gradient forces due to the near-field changes in density.

The recirculation is a critical issue for determining the large scale impact on the surrounding environment from the oxygenator when it is applied in the open sea. The recirculation around buoyant plumes in the ocean is poorly understood because previous studies, for example plumes from waste water outlets, have primarily focused on the dynamics and concentrations within the plume rather than the dynamical effects on the surroundings. The recirculation is therefore an important issue for future research on the effects from oxygenation. Also the possible dynamical coupling between the oxygenator intake in the surface layer and detrainment below may be important, in particular in shallow or enclosed areas or where the stratification is weak.

The role of pump rate, outlet depth and cross flow

In general, a doubling of the pump rate from 1 to 2 m^3 s^{-1} caused the simulated top level to change by about one meter, i.e. the plume reached one meter higher up in the water column in the case with largest pump rate (cf. Fig. 12). The detrainment was almost two times larger when the pump rate was doubled. These results show that the top level of the plume mainly is determined

by the local stratification rather than the flow rate, whereas the entrainment into the plume is relatively sensitive to the applied pump rate and, in this case, the detrainment rate scale proportional to the pump rate.

The distribution of the buoyant plume from oxygenation in the open sea may be affected by the far-field current field. The model simulations suggest that high current velocities would tend to bend the plume before it reaches its maximum top level. This behaviour can be compared to the influence from the atmospheric flow on plume dynamics, i.e. the bending of smoke from a chimney in strong winds. Numerical ocean studies also suggest a strong relationship between the horizontal velocity and the top level of a buoyant plume (Lavelle 1997) in accordance with experience obtained from laboratory studies (Turner 1979).

In the experimental setup, the oxygenator outlet at 17-m depth was located about 10 m above the bottom. If it were placed closer to the bottom a more direct impact from the oxygenator would be expected locally. Increased mixing between the water from the outlet and the surroundings could potentially be obtained if the outlet was placed in the bottom boundary layer very close to the bottom. In Sandöfjärden, the bottom boundary layer is expected to be relatively thin (~1 m) because of the small tidal forcing and the relatively weak bottom currents. However, the rhodamine experiment showed that the water from the oxygenator would mainly rise as a buoyant plume and therefore the expected direct effects from a lowering of the outlet would be concentrated locally around the oxygenator. Based on the operational experience with the Mixox oxygenators in lake systems, the outlet is normally located as high as possible in the water column. In applications with relatively high velocities in the pipe a shallow outlet will provide more space for additional mixing below the outlet and above the bottom. In principle, a deeper location of the outlet would increase the entrainment rates due to the larger density difference between the surface water and the deeper water, and this would imply a larger recirculation and therefore the indirect ventilation of the near bottom water would increase. The change in density between 17 m and the bottom is relatively small in Sandöfjärden but this effect may be important to consider in larger scale applications of oxygenation. If the outlet was placed too close the bottom, i.e. within a few meters, and with the current pump rates then temporary negative effects from increased resuspension of sediment would need to be taken into account. Such negative effects were not observed during the experiment. To achieve a certain pump capacity in a given area, a number of smaller pumps may therefore be more suitable than applying a single pump with a large pumping capacity.

Application of oxygenation on larger scales

The application of oxygenation on larger scales can be assessed by applying the results above on an idealized basin where the oxygen distribution is considered in two homogenous stationary layers. If the basin area is 3×2 km (approximately the size of the experimental area in Sandöfjärden) and the bottom layer is 10 m deep the transport of oxygen from an oxygenator would be given as: $F(O_2) = q(O_{2sur} - O_{2bot})$, where q is the pump rate of 1 m^3 s^{-1} and O_{2sur} and O_{2bot} is the surface and bottom oxygen concentrations, respectively. The surface concentration is assumed to be close to saturation, i.e. about 10 mg l^{-1}, and the bottom oxygen concentration is assumed to be about 3 mg l^{-1} (comparable to the conditions in Sandöfjärden, *see* also Fig. 3). Liikanen *et al*. (2002) find that the sediment oxygen demand of eutrophic lakes in Finland is about 0.5–1 g m^{-2} day^{-1}, and applying the lower value as representative for the oxygen demand in the idealized basin, this would imply total oxygen consumption in the bottom layer of 3000 kg day^{-1}. According to the flux estimate above, the transport of oxygen from an oxygenator to the bottom layer amounts to 605 kg day^{-1}, so about 5 oxygenators would provide enough oxygen to balance the microbial consumption. However, from the rhodamine experiment it is appearent that the oxygenation would initially affect the water below the pycnocline and therefore the oxygenated water would leave the area if not the basin is enclosed or otherwise have a limited exchange with the surroundings. This

could be the case in a coastal bay or fjord where there is no or limited exchange with the surroundings in the bottom layer. Thus, the local morphology has a large influence on the effect from oxygenation. These limitations on the oxygenation of bottom water also apply on larger regional scales if larger water bodies should be oxygenated. For example, if oxygenation of larger areas in the Baltic Sea is considered, then the local stratification around the oxygenators would determine the top level of the buoyant plume and also the local current field would have to be taken into account because the flow field could reduce the top level significantly. The oxygenation would then initially affect the water at the top level below the pycnocline. On longer time-scales (month–years), other effects would have to be considered because the influence from recirculation would then become important and eventually the effect from oxygenation would have a significant impact on the stratification.

Conclusions

The observed rhodamine distribution close to the pump demonstrated the potential for ventilating bottom water through artificial oxygenation and elucidated the convective motion and near-field dynamics. Water from the pump outlet rises as a buoyant plume and thereby entrains a significant amount of surrounding water in accordance with previous laboratory studies of convective motion. The rhodamine distribution showed that the lateral dispersion of the plume takes place in a thin few meter thick layer below the pycnocline. This demonstrates that large transports below the pycnocline can be sustained mechanically with a relatively small energy usage for pumping the surface water into the bottom layer. The method theoretically serves the possibility to oxygenate larger water areas with relatively small energy. However, in practice the success of this kind of artificial oxygenation will depend on the local conditions, e.g. on microbial oxygen consumption rate, stratification, season and basin morphology.

Entrainment of water in the rising buoyant plume led to a compensating recirculation in the model simulations and thereby generated a bottom circulation to the depth of the pipe outlet. However, the duration of the rhodamine release was too short to observe this in the field experiment.

A buoyant plume model was developed where entrainment was parameterized from differences in buoyancy between the plume and surrounding water and a free entrainment parameter was constrained from the observed distribution of rhodamine. The total detrainment from the plume was found to be about 7 times larger than the pump rate from the oxygenator. Mass distribution of rhodamine around the plume source and the lateral dispersion was simulated in accordance with observations. Model simulations showed that increased pumping caused a modest increase in the top level of the plume because this was mainly determined by the surrounding stratification. Corresponding simulations showed a high sensitivity to the cross flow velocities where the top level decreased significantly when the cross flow was increased from 0 to 0.3 m s^{-1}.

References

Choi K.W. & Lee J.H. 2007. Distributed entrainment sink approach for modeling mixing and transport in the intermediate field. *J. Hydraul. Eng.* 133: 804–814.

Gafsi M., Kettab A., Benmamar S. & Benziada S. 2009. Comparative studies of the different mechanical oxygenation systems used in the restoration of lakes and reservoirs. *J. Food Agr. Environ.* 7: 815–822.

Joye S. & Hollibaugh J.T. 1995. Influence of sulfide inhibition of nitrification on nitrogen regeneration in sediments. *Science*. 270: 623–625.

Lappalainen K.M. 1994. Positive changes in oxygen and nutrient contents in two Finnish lakes induced by Mixox hypolimnetic oxygenation method. *Verh. Int. Ver. Limnol.* 25: 2510–2513.

Lavelle J.W. 1995. The initial rise of a hydrothermal plume from a line segment source — results from a three-dimensional model. *Geophys. Res. Lett.* 22: 159–162.

Lavelle J.W. 1997. Buoyancy-driven plumes in rotating, stratified cross flows: Plume dependence on rotation, turbulent mixing, and cross-flow strength. *J. Geophys. Res.* 102: 3405–3420.

Lehtoranta J., Ekholm P. & Pitkänen H. 2008. Eutrophication driven sediment microbial processes can explain the regional variation in phosphorous concentration among the Baltic Sea sub-basins. *J. Mar. Syst.* 74: 495–504.

Liboriussen L., Søndergaard M., Jeppesen E., Thorsgaard I., Grünfeld S., Jakobsen T.S. & Hansen K. 2009. Effects of hypolimnetic oxygenation on water quality: results from five Danish lakes. *Hydrobiologia* 625: 157–172.

Liikanen A., Muroniemi T., Tankanen H., Väisänen T. & Martikainen P.J. 2002. Effects of temperature on greenhouse gas and nutrient dynamics in sediment of a eutrophic mid-boreal lake. *Biogeochemistry* 3: 269–286.

Luyten P.J., Jones J.E., Proctor R., Tabor A., Tett P. & Wild-Allen K. 1999. *COHERENS — A coupled hydrodynamical-ecological model for regional and shelf seas: user documentation*. Management Unit of the Mathematical Models of the North Sea.

McDougall T.J. 1978. Bubble plumes in stratified environments. *J. Fluid. Mech.* 85: 655–672.

McGinnis D.F., Lorke A., Wüest A., Stöckli A. & Little J.C. 2004. Interaction between a bubble plume and the near field in a stratified lake. *Water Resour. Res.* 40, W10206, doi:10.1029/2004WR003038.

Moshfeghi H., Etemad-Shahidi A. & Imberger J. 2005. Modelling of bubble plume destratification using DYRESM. *J. Water Supply Res. Technol. AQUA* 54.1: 37–46.

Pitkänen H., Kiirikki M., Savchuk O., Räike A., Korpinen P. & Wulff F. 2007. Searching efficient protection strategies for the eutrophied Gulf of Finland: The combined use of one-dimensional and three-dimensional modelling in assessing long-term state scenarios with high spatial resolution. *Ambio* 36: 272–279.

Stigebrandt A. & Gustafsson B.G. 2007. Improvement of the Baltic Proper water quality using large-scale ecological engineering. *Ambio* 36: 280–286.

Tuominen L., Heinänen A., Kuparinen J. & Nielsen L.P. 1998. Spatial and temporal variability of denitrification in the sediments of the northern Baltic Proper. *Mar. Ecol. Prog. Ser.* 172: 13–24.

Turner J. 1979. *Buoyancy effects in fluids*. Cambridge Univ. Press, Cambridge.

Wüest A., Brooks N.H. & Imboden D.M. 1992. Bubble plume modeling for lake restoration. *Water Resour. Res.* 28: 3235–3250.